A Compact Quadruple-Band Circular Polarized MIMO Antenna With Low Mutual Coupling

Asif Khan, Yejun He, *Senior Member, IEEE*, Zhou He, and Zhi Ning Chen, *Fellow, IEEE*

***Abstract*—This brief presents a compact multiband multiple input multiple output (MIMO) antenna, where two robot-character-shaped patches are closely positioned on the top of the substrate for circular polarization. The dimensions of the proposed MIMO antenna are 0.34λ × 0.13λ × 0.01λ at 4 GHz and the distance between two symmetrical elements is 0.05λ mm. The robot-character-shaped patch generates four different frequency bands of 3.85-4.25 GHz, 4.95-5.1 GHz, 6.94-7.35 GHz, and 8-8.3 GHz. The simulation and measurement results show that the designed antenna has better S-parameters $|S_{11}| \leq -10$ dB, and an isolation of $|S_{12}| \leq -25$ dB resulting from the irregular parasitic element to reduce mutual coupling, an axial ratio (AR) of no more than 3 dB, radiation pattern, total gain, and efficiency over all operating bands when compared to the existing two-port MIMO antennas. MIMO antennas diversity characteristics are also calculated to evaluate the proposed antennas performance. The proposed antenna is a good contender for 5G pioneer band, 5 GHz WLAN band, and satellite communication applications concomitantly.**

***Index Terms*—Multi-band antenna, multiple-input-multiple-output (MIMO) antenna, parasitic element, circular polarization, decoupling.**

I. Introduction

With the rapid advancement of wireless communication systems, higher transmission rate and larger channel capacity are highly desired to maintain the coverage area and obtain the high-definition (HD) video streaming without any interference [1]. Furthermore, MIMO antenna technology, which improves data rate without increasing input power or bandwidth [2], is one of the most vital features of future wireless communication systems. Although MIMO technology offers several advantages over competing technologies such as total gain and radiation efficiency, other characteristics of the MIMO antenna are reduced due to the compactness of multiple antennas [3]. Common isolation enhancement approaches including the isolation network [4], neutralization line [5], and defective ground structure (DGS) [6] have been discussed. Typical isolation enhancement approach such as decoupling structure attained an isolation improvement of 7-18 dB in [7]. Low mutual coupling between antenna elements is obtained by putting a multi-band antenna with PIN diodes and a dielectric resonator [8]. Apart from these isolation improvement strategies, the high isolation is achieved without introducing external decoupling structures in [9]. All of the structures previously documented have larger dimensions.

Several MIMO antenna designs were also proposed to cover different frequency bands for Wi-Fi, LTE, and WLAN applications with MIMO [10] and without MIMO [11] configuration. However, most of these MIMO antennas have a multi-layered 3-D configuration [10], very large in size [12], inadequate decoupling between MIMO components [13], limiting their applications for future compact, low-profile, and multi-band MIMO antennas.

Circularly polarized MIMO antennas have recently become very popular in wireless communication systems because they eliminate mutual coupling issues and the negative impact on overall system performance caused by combining multiple circularly polarized antennas to cover different frequency bands. Circular polarized (CP) antennas provide significant benefits over linear polarized antennas because reflected CP signals result in polarization reversal, therefore CP antennas are highly useful in fighting multi-path interference. As a result, following reflection, a right-hand circularly polarized (RHCP) incident signal will exhibit left-hand polarization (LHCP), which will be attenuated by an RHCP antenna. Furthermore, compared to linearly polarized antennas, circularly polarized antennas have better mobility, better alignment between transmitter and receiver, and better weather penetration [14]. The authors suggested a three-element compact MIMO antenna with polarisation (linear/circular) diversity in [15]. In [16], a dual-band MIMO antenna with polarization diversity is proposed. A circularly polarized dielectric-resonator (DR) two-port MIMO antenna (DRA) was proposed in [17], but it has limited isolation and a huge dimension, and operates at one band only. The designs in [18] have high isolation but suffer from the large size, small gain, narrow bandwidth, and Tri-band only.

The primary contributions of this research are as follows. i) Comparitive research is conducted to explain the originality of the proposed MIMO-CP antenna. In terms of size, bandwidth, axial ratio, gain, efficiency, isolation, and other MIMO

Manuscript received 28 July 2022; revised 30 August 2022 and 27 September 2022; accepted 4 October 2022. Date of publication 6 October 2022; date of current version 9 February 2023. This work was supported in part by the National Natural Science Foundation of China under Grant 62071306, and in part by the Shenzhen Science and Technology Program under Grant JCYJ20200109113601723, Grant JSGG20210420091805014, and Grant JSGG20210802154203011. This brief was recommended by Associate Editor K.-F. Tong. *(Corresponding author: Yejun He.)*

Asif Khan and Yejun He are with the Guangdong Engineering Research Center of Base Station Antennas and Propagation, the Shenzhen Key Laboratory of Antennas and Propagation, and the College of Electronics and Information Engineering, Shenzhen University, Shenzhen 518060, China (e-mail: asifm20019@gmail.com; heyejun@126.com).

Zhou He is with the Department of Mechanical Engineering, University of Maryland, College Park, MD 20742 USA (e-mail: zhe12@umd.edu).

Zhi Ning Chen is with the Department of Electrical and Computer Engineering, National University of Singapore, Singapore 117583 (e-mail: eleczn@nus.edu.sg).

Color versions of one or more figures in this article are available at https://doi.org/10.1109/TCSII.2022.3212618.

Digital Object Identifier 10.1109/TCSII.2022.3212618

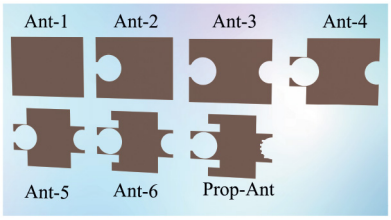

Fig. 1. Evolution process of the proposed antenna.

TABLE I
DIMENSIONS OF THE PROPOSED ANTENNA AND DECOUPLING STRUCTURE

Variable	Value(mm)	Variable	Value(mm)
l_1	12	l_6	2
l_2	4	r	3.2
l_3	4	a	11
l_4	2.2	b	1.5
l_5	7.5	c	2.5

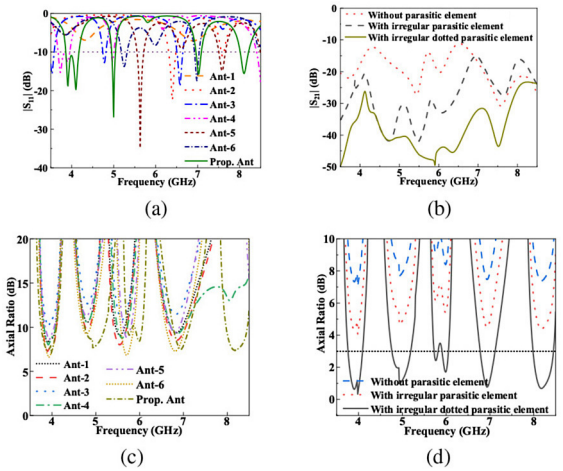

Fig. 2. (a) Simulated $|S_{11}|$ of all antennas, (b) simulated $|S_{21}|$, (c) axial ratio of all the iterative structures, and (d) axial ratio without/with parasitic element for the proposed antenna.

antenna aspects, the comparison indicates that the developed antenna outperforms the other designs. ii) To review, none of the proposals combine the advantages of a unique design, multi-band, high isolation, broadband CP characteristics, and MIMO capabilities in one set, such as our proposed design. To the best of the authors' knowledge, this brief is the first quad-band MIMO-CP antenna by executing the parasitic element and multi-band characteristic along with axial ratio less than 3 dB is obtained over entire operating bands.

II. DESIGN PROCESS OF THE ANTENNA

In this section, seven different designs have been simulated and compared with each other to obtain the desired multi-band antenna. And then, a novel robot-character-shaped MIMO antenna (the best one among all seven different designs in terms of their parameters) operating at four different frequencies is obtained. Finally, an irregular dotted parasitic element is placed between two identical patches for low mutual coupling and circular polarization.

A. MIMO Antenna Configuration

A rectangular monopole antenna is suggested (Ant-1). The radiator is cut off with a circle slot (Ant-2). Following that, another semicircle structure is loaded onto the 2nd iterative structure to create the 3rd, 4th, 5th, 6th, and then the proposed iterative structure is shown in Fig. 1. Dimensions of the proposed antenna are given in Table I.

Fig. 2(a) presents the reflection coefficient of all the extended iterative MIMO antennas. Ant-1 doesn't operate at any desired frequency as $|S_{11}| \geq -10$ dB. Ant-2 (6.5 GHz and 7.5 GHz), Ant-3 (4.7 GHz and 6.6 GHz), Ant-4 (4 GHz and 5 GHz), Ant-5 (5.6 GHz and 7.6 GHz), Ant-6 (5.2 GHz and 7 GHz) operate at two different frequencies due to the iterative structures $|S_{11}| \leq -10$ dB, followed by Ant-7 (proposed novel antenna) which operates at four center frequencies in three different frequency bands which are C-band, S-band, and X-band, respectively. Antenna-7 is slightly different from antenna-6 because of the small cuts in the circle which look like a jaw resulting in a quad-band antenna. The proposed MIMO antenna consists of two robot-character-shaped radiation patches where each patch is stimulated by a coaxial feed line from the ground plane and a parasitic element. The antennas in this MIMO context have the feed ports at different points, that's why it slightly affects $|S_{11}|$ and $|S_{22}|$ subsequently. The general assembly is designed on a widely available low-cost FR-4 substrate. The simulated and fabricated models are designed with dimensions of $0.34\lambda \times 0.13\lambda \times 0.01\lambda$ at 4 GHz. Two coaxial lines with 50 Ω are used to feed the two patches using lumped port excitation and the two patches are spaced by a small gap of 0.05 λ. High-frequency structure simulator software (HFSS) has been used for simulations.

B. Decoupling Structure Design and Analysis

High isolation between antennas is achieved in this strategy by adding a decoupling element. Dimensions of the decoupling structure are given in Table I. In this brief, an irregular dotted-shaped parasitic element has been used to obtain high isolation. Firstly, a rectangular shape is executed and supported by the other two sub-rectangular shapes which create an irregular shape. Due to this irregular-shaped decoupling structure, mutual coupling of $|S_{21}| \leq -20$ dB has been significantly reduced at two operating bands (3.85–4.25 GHz and 4.95–5.1 GHz). However, in other two operating bands (6.94–7.35 GHz and 8–8.3 GHz), $|S_{21}|$ remains above -20 dB which should be further reduced. Finally, the parasitic element is cut off with numerous small square-shaped holes, resulting in a reduced mutual coupling ($|S_{21}|$ and $|S_{12}| \leq -25$ dB) in the overall operating bands as shown in Fig. 2(b).

C. Axial Ratio

The parametric study of the axial ratio for the proposed MIMO antenna is studied from two perspectives (by the varying structure of the given antenna and by the addition of the different irregular structures). The AR of all the proposed structures is given in Fig. 2(c). It can be observed that the polarization is not affected by varying the structure of the antenna from a simple rectangular shape to a robotic shape.

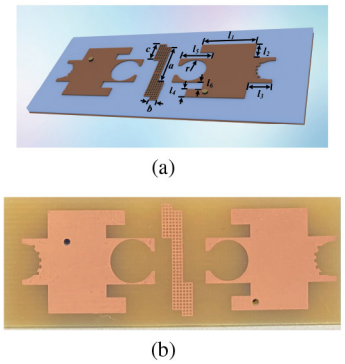

Fig. 3. (a) Simulated model and (b) fabricated model of the proposed antenna.

Actually, using different shapes of the irregular parasitic element will help to generate the circular polarization. As shown in Fig. 2(d), without any decoupling structure, the MIMO antenna doesn't work as a circularly polarized antenna. After appending the irregular structure, the value of axial ratio tends to 3 dB but the proposed MIMO antenna is still not circularly polarized as the AR $>$ 3 dB. Further modification in the structure (from an irregular structure to an irregular dotted structure) provides an AR band $<$ 3dB of 3.8-4.2 GHz, 4.75-5.2 GHz, 6.9-7.15 GHz, and 8-8.4 GHz, respectively. It is because the parasitic element with dots serves as a supplementary radiating source, which generates additional resonances in axial ratio bandwidth. This dotted slot influences the current distribution and the electric field.

D. Surface Current Distribution

Surface current distribution demonstrates the performance analysis of mutual coupling and other performance of the designed antenna over the desired frequency band and further justified. Fig. 4 depicts the current distributions utilized to analyze the circular polarization generation of the proposed antenna. Fig. 4(a) is a current scale. Fig. 4(b) and Fig. 4(c) illustrate the current distribution at 4 GHz, where the current is distributed on the patch-1 and the vector rotates clockwise when the phase is altered from 0° to 90°. As a result, the MIMO antenna could radiate LHCP in the broadside direction at 4 GHz. The same situation also happens when the antenna-1 is stimulated at 7 GHz, as illustrated in Fig. 4(f) and Fig. 4(g). Meanwhile, Fig. 4(d) and Fig. 4(e), Fig. 4(h) and Fig. 4(i) depict the antenna-1 being excited at 5 and 8 GHz, respectively. However, the vector turned anti-clockwise when the phase changed in this case.

III. Fabrication and Measured Results

Fig. 5 shows the proposed antenna's simulated and measured *S*-parameters and axial ratio. The simulated results are in good agreement with experimental measurements of the fabricated antenna. The MIMO antenna covers the frequency ranges of 3.85-4.25 GHz, 4.95-5.1 GHz, 6.94-7.35 GHz, and 8-8.3 GHz. The measured coupling values for the operational resonant bands at 4 GHz, 5 GHz, 7.05 GHz, and 8.17 GHz are less than −35 dB, −45 dB, −40.54 dB, and −26.5 dB, respectively, indicating that the MIMO antenna achieved high isolation. There is a slight deviation of *S*-parameters between

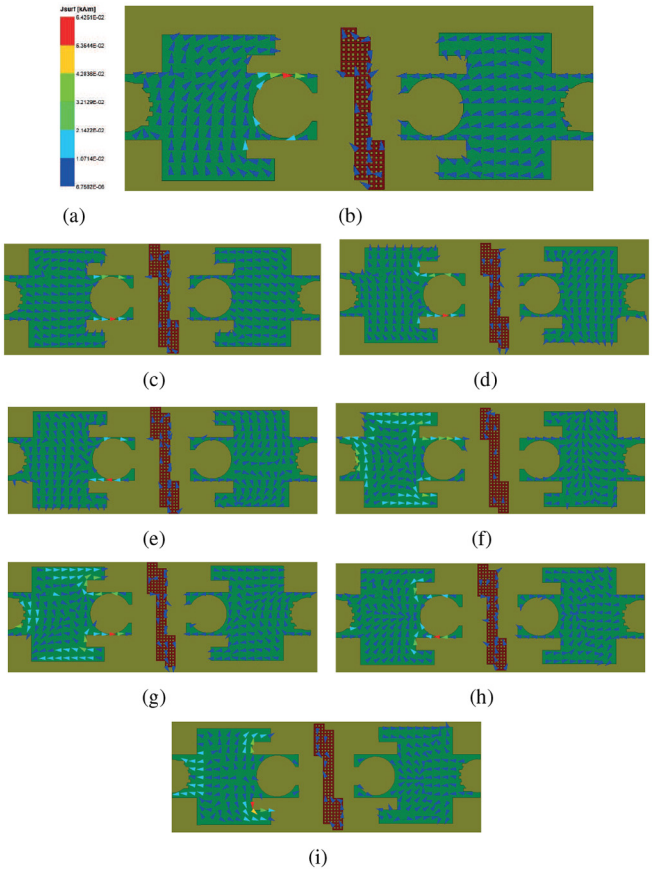

Fig. 4. Surface current distribution to generate CP currents excited by port-1, (a) current scale, (b) 4 GHz at 0°, (c) 4 GHz at 90°, (d) 5 GHz at 0°, (e) 5 GHz at 90°, (f) 7 GHz at 0°, (g) 7 GHz at 90°, (h) 8.1 GHz at 0°, (i) 8.1 GHz at 90°, respectively.

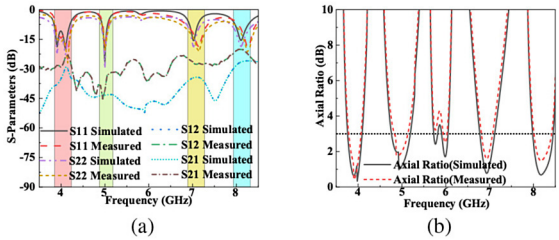

Fig. 5. Simulated and measured (a) *S*-parameters and (b) axial ratio.

simulation and measurement results due to manufacturing tolerance. Fig. 5 also shows the comparison between simulated and measured results of axial ratio as AR $\leq$ 3 dB within the antenna bandwidth.

The proposed MIMO antenna's simulated and measured radiation patterns for left hand circular polarization and right hand circular polarization in the four operating frequency bands are illustrated in Fig. 6. Due to cable connections and measurement errors, there is a small variation between the simulation and experimental results.

Simulated and measured gain and efficiency of the proposed antenna are shown in Fig. 7, where the gain is just above 4 dBi in the first and second band, 3 dBi in the third band, and above 5 dBi in the fourth operating band. Similarly, the radiation efficiency endures above 80% overall bands, respectively.

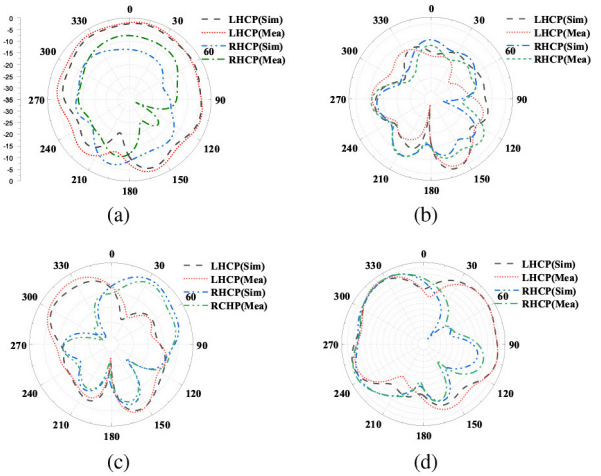

Fig. 6. Simulated and measured radiation patterns (LHCP and RHCP) of the proposed antenna at (a) 4 GHz, (b) 5 GHz, (c) 7 GHz, and (d) 8.1 GHz when port-1 is excited and port-2 is terminated.

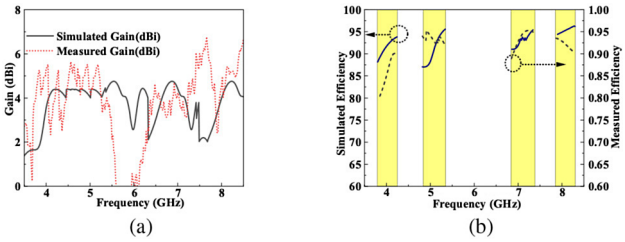

Fig. 7. Simulated and measured (a) gain and (b) efficiency of the proposed antenna.

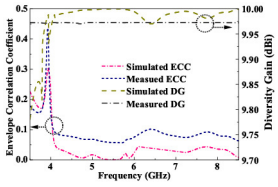

Fig. 8. Simulated and measured far field ECC and diversity gain.

IV. Diversity Characteristic Analysis

The ECC describes the amount of radiation pattern dependent between the two antenna components and shows the isolation between them. ECC may be calculated using far field as

$$\rho_e = \frac{|\int\int_{4\pi}[\vec{F}_1(\theta,\phi)\times\vec{F}_2(\theta,\phi)d\Omega]|^2}{|\int\int_{4\pi}[\vec{F}_1(\theta,\phi)]|^2\,d\Omega\,|\int\int_{4\pi}[\vec{F}_2(\theta,\phi)]|^2\,d\Omega} \quad (1)$$

where $\vec{F}_1(\theta,\phi)$ is far field of the MIMO array when port-1 is excited. The solid angle is denoted by Ω. Meanwhile, in contrast to a single antenna, the enhancement in multiple antennas' signal-to-noise ratio (SNR) is described by diversity. It can be calculated for a MIMO antenna as [20]

$$\mathrm{DG} = 10\sqrt{1-\beta} \quad (2)$$

In a MIMO system, larger channel capacity requires low ECC $\leq$0.5 [9], where ECC in the proposed MIMO antenna is less than 0.5 almost equal to 0 in all operating bands.

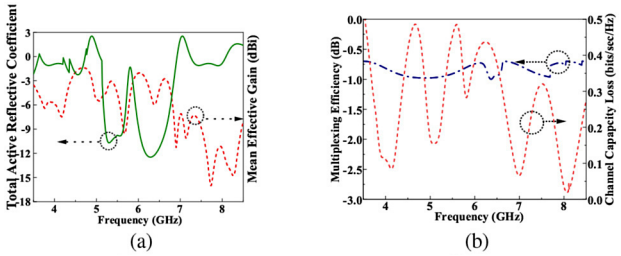

Fig. 9. Simulated (a) TARC and MEG, (b) multiplexing efficiency and channel capacity loss of the proposed MIMO antenna.

Similarly, low ECC leads to high diversity gain which shows good MIMO performance, as shown in Fig. 9(b).

The total active reflective coefficient (TARC) is a source that further describes the data rate and efficiency of the MIMO antenna. It can be given by [17]

$$\Gamma_a^t = \frac{\sqrt{\sum_{i=1}^{N}|h_i|^2}}{\sqrt{\sum_{i=1}^{N}|g_i|^2}} \quad (3)$$

where $|g_i|$and $|h_i|$ are the incident signals and reflected signals, respectively. The value of TARC $\leq$ 0 means that the whole amount of power is radiated competently, where this designed antenna value of TARC is less than zero in all operating bands as shown in Fig. 9(a).

The suggested MIMO antenna's multiplexing efficiency was computed using the following relation [9].

$$\eta_{Mux} = \sqrt{1-|\rho|^2}\eta_1\eta_2 \quad (4)$$

where η_1, η_2 and ρ denote the efficiency of element-1, the efficiency of element-2, and the complex envelope correlation coefficient ($\rho \approx |\mathrm{ECC}|^2$) between the two elements. As shown in Fig. 9(b), η_{Mux} for all operating bands ≥ -1dB, which is reasonable for a MIMO operation.

Mean effective gain (MEG) evaluates the function of the MIMO antenna in a wireless environment. It can be calculated by using S-parameters as

$$\mathrm{MEG} = \frac{(1-|S_{ii}|^2-|S_{ij}|^2)}{(1-|S_{ij}|^2-|S_{jj}|^2)} \quad (5)$$

The value of MEG $\leq$ 3 dB shows a better MIMO antenna performance [17]. The simulated MEG of the proposed MIMO antenna is given in Fig. 9(a). It can be noticed the value is smaller than 3dB, which means that the projected antenna has improved diversity parameter.

The CCL provides information about the upper limit of the communication that can be flourished executed without any loss. CCL can be determined by

$$\mathrm{CCL} = \log_2 Det(a^i) \quad (6)$$

$$a^i = \begin{bmatrix} a_{ii} & a_{ij} \\ a_{ji} & a_{jj} \end{bmatrix} \quad (7)$$

$$a_{ii} = 1-(|S_{ii}|^2+|S_{ji}|^2) \quad (8)$$

$$a_{jj} = 1-(|S_{jj}|^2+|S_{ij}|^2) \quad (9)$$

$$a_{ij} = (S_{ii}*S_{ij})+(S_{ji}*S_{jj}) \quad (10)$$

$$a_{ji} = (S_{jj}*S_{ji})+(S_{ij}*S_{ii}) \quad (11)$$

TABLE II
COMPARISON TO OTHER TWO-PORT MIMO ANTENNAS

	[16]	[17]	[19]	[20]	This work
Number of operating bands	2	1	2	1	4
Bandwidth (GHz)	2.4-2.7, 4.9-5.6	5.7-8.2	2.4-2.5, 5.1-5.3	5.48-5.52	3.8-4.2, 4.9-5.1, 6.9-7.3, 8-8.3
Maximum ECC	0.05, 0.001	0.05	0.2, 0.4	0.05	0.001, 0.001, 0.002, 0.005
Minimum $\|S_{21}\|$ (dB)	-35, -45	-15	-20, -20	-34	-35, -45, -40, -26.5
Polarization	CP	CP	NA	NA	CP
Compactness (Length, width, height) (mm)	70 70 1.524	80 80 1.6	55 50 1.6	NA	53 20 1.6
Decoupling Technique	Ground structure	Metal strip on the DRAs	Trans-mission line	Meta-material absorber	Parasitic element

where CCL $\leq$ 0.5 bits/sec/Hz is considered for an enhanced MIMO antenna performance. As shown in Fig. 9(b), the value of CCL $\leq$ 0.15 bits/sec/Hz is attained overall resonant points.

In Table II, the performance of the proposed two-port MIMO antenna is compared with that of the previous works. It is obvious that our MIMO antenna is better with regard to the size, multiband operation, isolation, maximum ECC, and polarization.

V. CONCLUSION

A two-element compact and low-cost robot-character-shaped multi-band MIMO-CP antenna is proposed. Initially, several designs were supposed to achieve a quadruple band antenna, which operated at four different frequency bands of 3.95–4.25 GHz, 4.95-5.1 GHz, 6.94-7.35 GHz, and 8-8.3 GHz, respectively. Finally, the high isolation of $|S_{21}| \leq -25$ dB in all four operating bands is achieved due to the design of an irregular dotted-shaped parasitic element between two patches. Diversity characteristics were also examined and better results were achieved in terms of DC, ECC, TARC, MEG, and CCL. The proposed MIMO antenna has been simulated and measured successfully, and the results show that the proposed MIMO antenna is a suitable candidate for 5G pioneer band, 5 GHz WLAN band, and satellite communication applications.

REFERENCES

[1] Q. Rubani, S. H. Gupta, and A. Rajawat, "A compact MIMO antenna for WBAN operating at Terahertz frequency," *Optik*, vol. 207, pp. 1–9, Apr. 2020.

[2] W. Hong, "Solving the 5G mobile antenna puzzle: Assessing future directions for the 5G mobile antenna paradigm shift," *IEEE Microw. Mag.*, vol. 18, no. 7, pp. 86–102, Nov./Dec. 2017.

[3] M. S. Sharawi, "Printed multi-band MIMO antenna systems and their performance metrics [Wireless Corner]," *IEEE Antennas Propag. Mag.*, vol. 55, no. 5, pp. 218–232, Oct. 2013.

[4] J. Baek and J. Choi, "The design of a LTE/MIMO antenna with high isolation using a decoupling network," *Microw. Opt. Technol Lett.*, vol. 56, no. 9, pp. 2187–2191, Sep. 2014.

[5] S. Su, C. Lee, and F. Chang, "Printed MIMO-antenna system using neutralization-line technique for wireless USB-dongle applications," *IEEE Trans. Antennas Propag.*, vol. 60, no. 2, pp. 456–463, Feb. 2012.

[6] A. Khan, S. Geng, X. Zhao, Z. Shah, M. U. Jan, and M. A. Abdelbaky, "Design of MIMO antenna with an enhanced isolation technique," *Electronics*, vol. 9, no. 8, pp. 1–17, Jul. 2020.

[7] T. Pei, L. Zhu, J. Wang, and W. Wu, "A low-profile decoupling structure for mutual coupling suppression in MIMO patch antenna," *IEEE Trans. Antennas Propag.*, vol. 69, no. 10, pp. 6145–6153, Oct. 2021.

[8] Y. I. Abdulraheem et al., "Design of frequency reconfigurable multiband compact antenna using two PIN diodes for WLAN/WiMAX applications," *IET Microw. Antennas Propag.* vol. 11, no. 8, pp. 1098–1105, Jun. 2017.

[9] F. Wang, Z. Duan, X. Wang, Q. Zhou, and Y. Gong, "High isolation millimeter-wave wideband MIMO antenna for 5G communication," *Int. J. Antennas Propag.*, vol. 2019, pp. 1–12, May 2019.

[10] W. Han, X. Zhou, J. Ouyang, Y. Li, R. Long, and F. Yang, "A six-port MIMO antenna system with high isolation for 5-GHz WLAN access points," *IEEE Antennas Wireless Propag. Lett.*, vol. 13, pp. 880–883, Mar. 2014.

[11] Y. Liu, H.-H. Kim, and H. Kim, "Loop-type ground radiation antenna for dual-band WLAN applications," *IEEE Trans. Antennas Propag.*, vol. 61, no. 9, pp. 4819–4823, Sep. 2013.

[12] A. MoradiKordalivand, T. A. Rahman, and M. Khalily, "Common elements wideband MIMO antenna system for WiFi/LTE access-point applications," *IEEE Antennas Wireless Propag. Lett.*, vol. 13, pp. 1601–1604, Mar. 2014.

[13] M. Ikram, M. S. Sharawi, and A. Shamim, "Compact circular connected monopole antenna arrays for wideband MIMO applications," *IET Microw. Antennas Propag.*, vol. 12, no. 13, pp. 2122–2127, Oct. 2018.

[14] D. M. Pozar and S. M. Duffy, "A dual-band circularly polarized aperture-coupled stacked microstrip antenna for global positioning satellite," *IEEE Trans. Antennas Propag.*, vol. 45, no. 11, pp. 1618–1625, Nov. 1997.

[15] Y. Sharma, D. Sarkar, K. Saurav, and K. V. Srivastava, "Three-element MIMO antenna system with pattern and polarization diversity for WLAN applications," *IEEE Antennas Wireless Propag. Lett.*, vol. 16, pp. 1163–1166, May 2017.

[16] L. Malviya, R. K. Panigrahi, and M. V. Kartikeyan, "A 2×2 dual-band MIMO antenna with polarization diversity for wireless applications," *Progr. Electromagn. Res. M*, vol. 61, pp. 91–103, Jan. 2016.

[17] G. Varshney, R. Singh, V. S. Pandey, and R. S. Yaduvanshi, "Circularly polarized two-port MIMO dielectric resonator antenna," *Progr. Electromagn. Res. M*, vol. 91, pp. 19–28, Apr. 2020.

[18] K. Babu and B. Anuradha, "Tri-band MIMO antenna for WLAN, WiMAX and defence system and radio astronomy applications," *Adv. Electromagn.*, vol. 7, no. 2, pp. 60–67, Mar. 2018.

[19] J. Deng, J. Li, L. Zhao, and L. Guo, "A Dual-band inverted-F MIMO antenna with enhanced isolation for WLAN applications," *IEEE Antennas Wireless Propag. Lett.*, vol. 16, pp. 2270–2273, Jun. 2017.

[20] P. Garg and P. Jain, "Isolation improvement of MIMO antenna using a novel flower shaped metamaterial absorber at 5.5 GHz WiMAX band," *IEEE Trans. Circuits Syst. II, Exp. Briefs*, vol. 67, no. 4, pp. 675–679, Apr. 2020.